Composites Science and Technology 112 (2015) 8–15

Contents lists available at ScienceDirect

Composites Science and Technology

journal homepage: www.elsevier.com/locate/compscitech

Exploration of the potential for pseudo-ductility in thin ply CFRP angle-ply laminates via an analytical method

J.D. Fuller *, M.R. Wisnom

Advanced Composites Centre for Innovation and Science, University of Bristol, Queen's Building, Bristol BS8 1TR, United Kingdom

ARTICLE INFO

Article history:
Received 18 October 2014
Received in revised form 25 February 2015
Accepted 28 February 2015
Available online 10 March 2015

Keywords:
A. Laminate
B. Non-linear behaviour
B. Plastic deformation
C. Modelling
C. Laminate theory

ABSTRACT

Thin ply laminates have shown much promise in recent times in terms of their exciting damage suppression characteristics. Utilisation of this damage suppression in carbon–epoxy angle-ply laminates has been shown experimentally to yield a highly non-linear stress–strain response. This paper presents an analytical modelling method that incorporates matrix plasticity and reorientation of the fibres into a classical laminate analysis for the prediction of the in-plane response of thin ply angle-ply laminates. It is shown that the method can successfully predict the non-linear behaviour of $[\pm\theta_5]_s$ laminates with values of θ between 15° and 45°. The main characteristics of the stress–strain curve, such as the initial largely linear region, yield point and stiffening before final failure, are all well captured. The modelling has allowed straightforward identification of a particular fibre angle that exhibits strength in excess of 900 MPa, strain to failure of more than 3.5% and a promising pseudo-ductile strain of 1.2%.

1. Introduction

Thin ply carbon fibre reinforced polymer (CFRP) composites have recently been shown to exhibit superior damage suppression characteristics compared to laminates consisting of standard thickness plies. Application of tow spreading technology [1,2] has allowed plies of a thickness lower than the standard 0.125 mm to be manufactured reliably. Spread-tow materials have shown that the onset of matrix cracking and delaminations can be delayed or even prevented completely [2–9] leading to increased strength and strain to failure. The results in all cases are promising and show that the composites design space can be expanded, maximising properties. Guillamet et al. [3] studied the effects of ply clustering on thin ply non-crimp fabric laminates. Monitoring of the free edge of each specimen showed that damage in the form of matrix cracking and delaminations (both free-edge and initiated from matrix cracking) occurred in the clustered regions. This damage was, in all cases, lessened or even suppressed in the region containing distributed thin plies. Amacher et al. [7] also show via ultrasonic C-scan and acoustic emission that thin ply quasi-isotropic (QI) laminates, tested under uniaxial tension and open-hole fatigue, again delay or even remove matrix cracking and delaminations prior to failure. In-depth investigations of both in-plane and out-of-plane behaviour of thin ply QI laminates have been conducted by Yokozeki et al. [4,10]. It was found that, when compared to laminates with thicker plies of the same material (ply thickness, $t_p = 0.14$ mm), the thin ply specimens ($t_p = 0.07$ mm) exhibited considerably less damage at the same load. This suppression of damage, however, has not always been beneficial. Arteiro et al. [8,9] and Sihn et al. [2] both found that thin ply laminates exhibited lower notched strength than laminates with thicker plies. It was concluded that the stress relaxation mechanisms of matrix cracking and splitting were inhibited, resulting in a lower failure stress.

These studies concentrate on comparing the damage onset and final failure in laminates exhibiting linear elastic stress–strain behaviour and as such brittle failures are predominant. Achieving some non-linear behaviour is desirable, as this further extends the design allowables for thin ply composites. The non-linear behaviour can be thought as a pseudo-ductility and a parameter to describe the extent of this, pseudo-ductile strain, ϵ_d, can be defined as the failure strain minus the strain at the same stress level on a straight line of initial modulus. One way of achieving non-linearity is to use an angle-ply laminate, with all plies oriented at an angle to the loading direction, $[\pm\theta_n]_s$. These laminates have shown the potential to reach high strains [15], but are often limited by premature failures driven by free-edge delaminations. Herakovich [15] investigated these edge effects using $[(+\theta/-\theta)_2]_s$ and $[+\theta_2/-\theta_2]_s$ laminates, where $\theta = 10°, 30°, 45°$. All laminates with dispersed standard thickness plies exhibited improved strength and strain to failure compared with blocked ply laminates, which, for the

* Corresponding author.
E-mail address: j.d.fuller@bristol.ac.uk (J.D. Fuller).

http://dx.doi.org/10.1016/j.compscitech.2015.02.019
0266-3538/

30° and 45° laminates, allowed non-linear behaviour to develop further. Reducing the ply thickness further, Ogihara and Nakatani [6] presented work on thin ply carbon–epoxy angle-ply laminates. Specimens of ±45° not only showed increases in tensile strength with a ply thickness of 0.05 mm ($[\pm\theta_{12}]_s$) rather than 0.15 mm ($[\theta_4/-\theta_4]_s$), but also showed much more non-linearity, with around 8 times higher strain to failure.

More recently, thin ply angle-ply laminates have been shown by the authors to exhibit highly non-linear behaviour and suppress damage until final failure [14]. It has been demonstrated that, with laminates of $[\pm\theta_5]_s$ ($\pm 20^\circ \leqslant \theta \leqslant \pm 45^\circ$), a respectable initial modulus can be achieved alongside large pseudo-ductile strains. For example, $[\pm 25_5]_s$ laminates reached a mean strength of 950 MPa, pseudo-ductile strain of 1.22%, whilst retaining an initial modulus of 39 GPa. For a loss of strength of only 21%, $[\pm 30_5]_s$ laminates exhibited considerably more pseudo-ductile strain, with a mean value of 3.10%. Matrix cracking and delaminations were effectively suppressed, allowing the fibres to reorient towards the loading direction and the development of matrix plasticity. Fibre rotation is integral to the response of these laminates, which both Wisnom [11] and Herakovich et al. [12] have emphasised in work on accurately representing the stress state in $[\pm 45_n]_s$ laminates.

Herakovich et al. [12] modelled the damage evolution using a continuum damage mechanics model proposed by Ladeveze and LeDantec [13] that is then coupled with fibre rotation to show the effect reorientation of the fibres has on the overall stress–strain behaviour. The model approximates the laminate stiffness loss to matrix cracking and fibre–matrix debonding in order to define damage variables that attempt to describe the damage development. While this modelling approach is concentrated on the progression of damage, Sun and Chen devised a simple orthotropic plasticity model to describe the non-linear behaviour of composites [16]. This straightforward approach assumes linear elastic behaviour in the fibre direction and an elastic–plastic matrix to model the non-linearity of the composite with a single orthotropy parameter. A study performed by Winn and Sridharan [19] to investigate the accuracy of this approach concluded that predictions were accurate except for cases involving large amounts of matrix cracking.

In this paper, analytical modelling of thin ply angle-ply CFRP laminates is presented. The modelling incorporates fibre rotation and uses the Sun and Chen single-parameter plasticity model [16] to define the non-linearity of the composite. The results are validated using the experimental results presented in [14]. The potential of these laminates to produce non-linear behaviour with high strength, pseudo-ductility and large strains to failure is then explored. Note that, in this paper, $[+\theta/-\theta]_{ns}$ is denoted $[\pm\theta_n]_s$.

2. Modelling procedure

The orthotropic plasticity model proposed by Sun and Chen [16] has been chosen to simulate the non-linear behaviour of the composite. This choice is verified by the evidence from X-ray computed tomography scans and micrographs presented in [14] that show damage has been suppressed until final failure of the specimens. In all of the layups tested, delaminations do not occur and in all but one ($[\pm 45_5]_s$) matrix cracking is completely absent. Investigations of the fibre–matrix interface were not conducted, though it is unlikely that considerable debonding occurred at the microscale, as the stress perpendicular to the fibres (σ_{22}) is compressive in the laminates tested. This damage-free state allows a modelling approach based solely on the plasticity of the matrix, rather than damage mechanics, which also incorporates matrix cracking and delamination. Fibre rotations are then accounted for via the relationship between the original fibre angle, θ and the longitudinal and transverse strains, ϵ_x and ϵ_y respectively. This gives rise to a non-linear, iterative analytical model based on Classical Laminate Analysis (CLA), programmed in Matlab. Initially a micromechanical model [17] that treats the constituent fibre and matrix as an elastic–plastic material, is used to identify the plastic behaviour of the matrix. Due to the complexity of the micromechanical approach, however, it is solely used as a tool to define parameters for the orthotropic plasticity model. The next stage of the process models the uniaxial tensile behaviour of an angle-ply laminate, incorporating the previously determined matrix properties. The plasticity modelling is described in detail within [16,17], so only the key elements and assumptions of each stage of the method shall be highlighted at this point. The chosen material is a spread tow carbon fibre-epoxy prepreg manufactured by SK Chemicals, designated Skyflex USN020A, as used in [14]. The constituents are Mitsubishi-Rayon TR30 carbon fibres and SK Chemicals proprietary semi-toughened epoxy resin, K50. The material was shown in [14] to have a relatively low fibre volume fraction of 42%. The cured ply thickness of this material is 0.03 mm.

2.1. Micromechanical model

The micromechanical model is utilised to define the plastic properties of the matrix material. Incremental solutions of the fibre and resin compliance matrices are found and then combined to give the tensile response of a unit cell of the composite. The unit cell of material is idealised, as shown in Fig. 1, as a square cross-section of fibre (region AF), bounded by two regions of matrix (AM and B). This area forms a quarter-model of the fibre and matrix, assuming a rectangular distribution of fibres in the composite. The arrangement, including sizing the square fibre cross-section to be equivalent to the actual circular cross-section, has been maintained from [17]. This was deemed sufficient to allow the parameters required for the model to be established in a straight-forward manner. The fibre region is assumed to be orthotropic linear-elastic and the matrix isotropic elastic–plastic, following the von Mises J_2-flow rule. This flow rule assumes an isotropic hardening that is independent of hydrostatic pressure. Despite the epoxy matrix being a pressure dependent material, simplification of the modelling in this respect should not lead to large inaccuracies when the laminates are loaded under uniaxial tension. The respective material properties used in the model are set out in Table 1. The transverse, E_{22}, and shear, G_{12}, moduli of the fibre have been estimated via knowledge of the longitudinal fibre modulus, E_{11}, (from Mitsubishi-Rayon TR30 fibre data [20]) and unidirectional composite stiffness matrix, $[Q]$. A value of $E = 3.3$ GPa for the K50 matrix material is found from the rules of mixtures via knowledge of the fibre volume fraction and E_{11} of the material. The remaining elastic constants, G and ν, are given

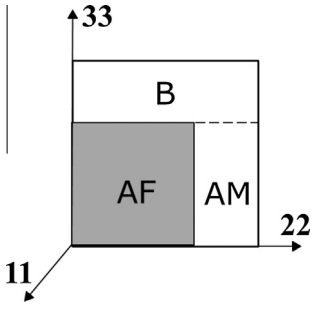

Fig. 1. Representation of the unit cell of composite used to determine the matrix plasticity. Region AF indicates fibre assumed to have a square cross-section, AM and B refer to the surrounding matrix material.

Table 1
Fibre and matrix material properties, as used in the micromechanical model.

	Fibre (TR30)		Matrix (K50)
E_{11} [GPa]	235	E [GPa]	3.3
E_{22} [GPa]	13		
G_{12} [GPa]	15	G [GPa]	1.2
ν_{12}	0.2	ν	0.38

by the relationship between E, G and ν for an isotropic material. The values of E_{22} and G_{12} for the fibre and G and ν for the matrix are adjusted until the values of [Q] matched those already determined for the Skyflex material from material characterisation testing, found in [14]. A state of plane stress is also assumed to exist perpendicular to the x–y (1–2) plane, leading to $\sigma_{33} = \sigma_{23} = \sigma_{13} = 0$. Where the x-direction is the direction of loading and y-direction is the transverse in-plane direction. The material principal directions of 11, 22, 33 are the fibre, in-plane transverse and through-thickness directions respectively.

The assumptions of plane stress and linear-elastic fibres allows the plastic potential function, f, to be written as:

$$f = \frac{1}{2}\left(\sigma_{22}^2 + 2a_{66}\sigma_{12}^2\right) \tag{1}$$

The effective stress, $\bar{\sigma}$, is related to Eq. (1) as follows:

$$\bar{\sigma} = \sqrt{3f} = \left[\frac{3}{2}\left(\sigma_{22}^2 + 2a_{66}\sigma_{12}^2\right)\right]^{0.5} \tag{2}$$

The plastic behaviour of the matrix is described by the effective plastic strain, $\bar{\epsilon}_M^p$, and effective stress, $\bar{\sigma}_M$, which are related via a power law,

$$\bar{\epsilon}_M^p = \beta(\bar{\sigma}_M)^n \tag{3}$$

The β and n terms are determined via the stress–strain curve produced by the tensile test of $[90]_{16}$ laminates. Where $\theta = 90^\circ$, Eq. (7) reduces to (8), allowing the determination of $h(\theta)$ (the parameter that relates the effective plastic stress and strain in the θ direction to global applied stress and plastic strain) without requiring the unknown material orthotropy constant, a_{66}. Where $h(\theta)$ is found using the plastic potential function in Eq. (1) and substituting for the terms of the stress transformation matrix.

$$\sigma_{11} = \cos^2\theta\sigma_x \tag{4}$$

$$\sigma_{22} = \sin^2\theta\sigma_x \tag{5}$$

$$\sigma_{12} = -\sin\theta\cos\theta\sigma_x \tag{6}$$

Leading to:

$$h(\theta) = \left[1.5(\sin^4\theta + 2a_{66}\sin^2\theta\cos^2\theta)\right]^{1/2} \tag{7}$$

$$h(\theta) = [1.5]^{1/2} \tag{8}$$

This allows computation of the experimental $\bar{\epsilon}_M^p$ and $\bar{\sigma}_M$ via Eqs. (9) and (10):

$$\bar{\sigma}_M = h(\theta)\sigma_x \tag{9}$$

$$\bar{\epsilon}_M^p = \epsilon_x^p / h(\theta) \tag{10}$$

Initial values of β and n are found, using Eq. (3), and provide starting points for describing the plastic strain increments in the matrix regions (AM and B) within the model. The parameters β and n are then adjusted within the micromechanical model to give a stress–strain response that closely matches the experimental 90° results, as shown by Fig. 2. The final values of $\beta = 3.5 \times 10^{-33}$ and $n = 3.86$ were used to produce this curve fit. Fig. 2a shows that these parameters are certainly valid up to the strain to failure of the 90° specimens and is also extrapolated beyond this to show the behaviour at higher strains.

The following step is to produce off-axis stress–strain curves over a range of fibre angles from 10° — 60°, as shown in Fig. 2b. The same unit cell approach is maintained, whilst the fibre is oriented at an angle, θ, to the loading direction. Employing Eq. (7), and setting an initial value of $a_{66} = 1$, the $\bar{\epsilon}_M^p$ and $\bar{\sigma}_M$ for each fibre angle can be calculated. It is necessary to determine a single value of a_{66} for the laminate-level plasticity model. Sun and Chen [17] show, using a composite of boron/aluminium, that one value of a_{66} can collapse the effective stress-plastic strain ($\bar{\sigma} - \bar{\epsilon}^p$) curves of each off-axis unit cell on to the curve produced by the micromechanical model for the 90° unit cell. Fig. 2c demonstrates that the same is applicable for the Skyflex USN020A material, showing that the method can adequately represent the plastic behaviour of this material.

2.2. One-parameter orthotropic plasticity model

The simple one-parameter plasticity model presented by Sun and Chen [16] also assumes that non-linearity in the fibre direction is negligible; with all the plasticity originating from the transverse and in-plane shear stresses. In this respect, the model is well suited to implementation with angle-ply laminates, as the transverse and shear stresses interact and can be modelled with the plastic potential function given by Eq. (1).

A state of plane stress is deemed to exist and the material is assumed to remain orthotropic throughout — allowing the use of a constant value of a_{66}. The plastic behaviour of the composite is again defined by a power law, relating effective plastic strain, $\bar{\epsilon}^p$, and effective stress, $\bar{\sigma}$,

$$\bar{\epsilon}^p = A(\bar{\sigma})^r \tag{11}$$

where A and r are calculated from performing a regression analysis in order to fit a power law curve to the effective stress-plastic strain produced by the micromechanical model, as shown by the black line in Fig. 2c. This process leads to values of $A = 5.5 \times 10^{-32}$, $r = 3.579$ and $a_{66} = 2.15$ to be used to describe the plastic behaviour. Knowledge of the plastic parameters allows the laminate solution to be found by relating the incremental strains and stresses,

$$\{d\epsilon\} = [S]\{d\sigma\} \tag{12}$$

The compliance matrix, [S], can be inverted to give the reduced stiffness matrix, [Q]. This consists of elastic, $[Q_e]$ and plastic, $[Q_p]$ contributions that make up the overall response of each ply in the laminate and, from Sun and Yoon [18], are related in the following way:

$$[S]^{-1} = [Q] = [Q_e] - [Q_p] \tag{13}$$

The $[Q_p]$ is defined as shown below:

$$[Q_p] = [Q_e]\frac{\frac{\partial f}{\partial\{\sigma\}}\left(\frac{\partial f}{\partial\{\sigma\}}\right)^T[Q_e]}{\frac{4}{9}\bar{\sigma}^2 H_p + \left(\frac{\partial f}{\partial\{\sigma\}}\right)^T[Q_e]\frac{\partial f}{\partial\{\sigma\}}} \tag{14}$$

The plastic modulus, H_p, is defined as:

$$H_p = \frac{d\bar{\sigma}}{d\bar{\epsilon}^p} \tag{15}$$

The plastic potential function, f, is expressed with respect to stress and takes the vector form:

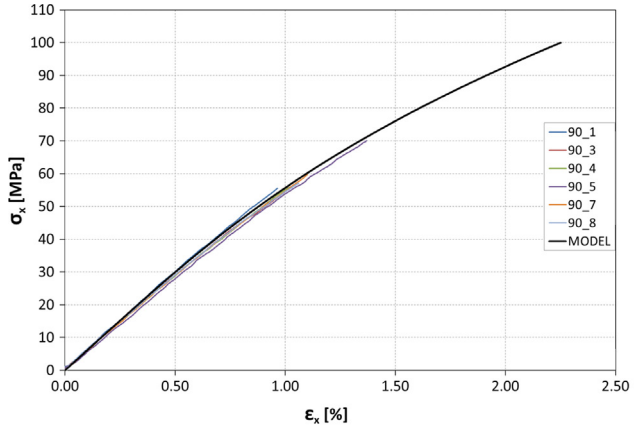

(a) Experimental $[90]_{16}$ with model fit.

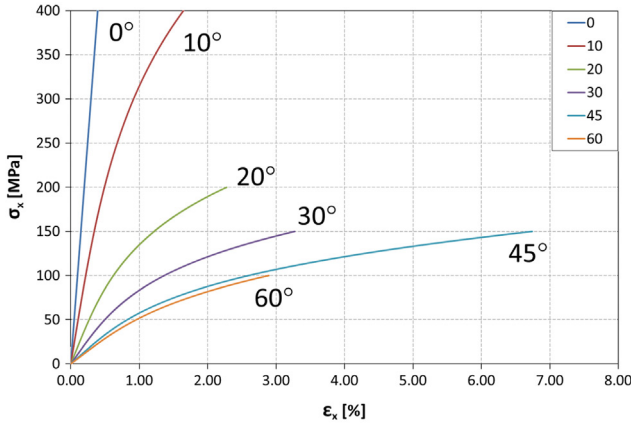

(b) Off-axis model results (0° — 60°).

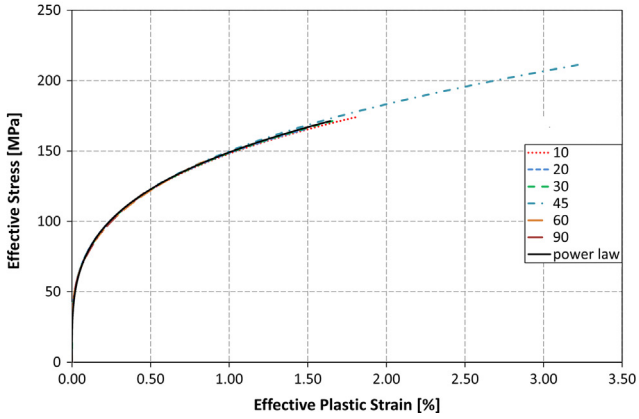

(c) Off-axis $\bar{\sigma}$-$\bar{\epsilon}^p$ curves.

Fig. 2. Micromechanical modelling steps to find *A* and *r*.

$$\frac{\partial f}{\partial\{\sigma\}} = \begin{Bmatrix} 0 \\ \sigma_{22} \\ 2a_{66}\sigma_{12} \end{Bmatrix} \tag{16}$$

2.3. Fibre rotations

Fibre rotation is incorporated into the model and assumed to take place as a 'scissoring' action, as described in [11,12,14]. The fibres are treated as inextensible and modelled as rotating towards the direction of loading. The updated 'rotated' fibre angle, θ', is related to the longitudinal and transverse strains, ϵ_x and ϵ_y and defined as:

$$\theta' = \arctan\left\{\frac{\tan(\theta) + \epsilon_y}{1 + \epsilon_x}\right\} \tag{17}$$

2.4. Definition of pseudo-ductility

Pseudo-ductility, in this case, arises from the geometric effect of fibre reorientation as well as yielding of the matrix that allow further non-linear strains to be taken by the laminate. Analogous to proof stress, the "yield stress", σ_Y, is defined as the point of intersection between the laminate stress–strain curve and a straight line of the initial modulus offset by 0.1% strain (a value commonly used to determine proof stress). The pseudo-ductile strain, ϵ_d, is the failure strain minus the strain at the same stress level on a straight line of initial modulus. To aid understanding, these parameters are presented graphically in Fig. 3.

2.5. Laminate modelling process

As aforementioned the one-parameter plasticity model is contained within an iterative, non-linear CLA solution. The compliance

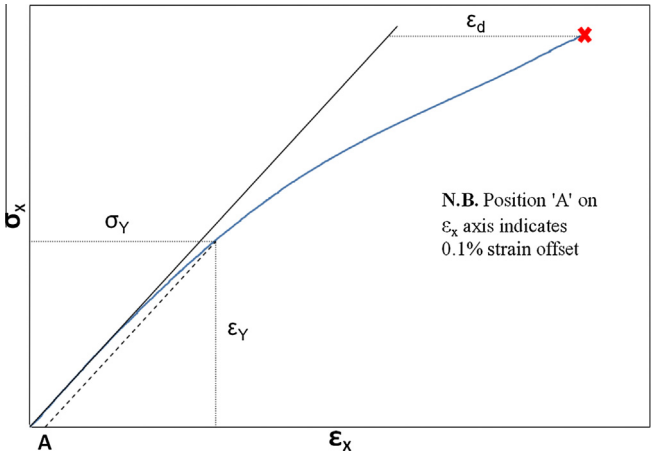

Fig. 3. The parameters of "yield" stress, σ_Y, and pseudo-ductile strain, ϵ_d, are presented for a typical stress–strain response.

matrix, [S], is updated at each loading increment, allowing the change in ply stiffness, caused by the reorientation of fibres and matrix plasticity, to be accounted for. Following the upload of material properties and stacking sequence from input files, the general process the model undertakes each loading increment is presented in Fig. 4.

Failure of the laminate is based on a maximum strain criterion – selected due to the large non-linearities demonstrated experimentally and the subsequent inability of the maximum stress or Tsai–Wu criteria to adequately represent the laminate failure. Experimentally obtained values, determined from characterisation tests of $[0_{16}]$, $[90_{16}]$ and $[\pm 45_5]_s$ specimens, as described in [14], for the strain to failure in the three principal material directions are as follows: $\epsilon_{11} = 1.5\%; \epsilon^t_{22} = 1.1\%; \epsilon^c_{22} = -10\%; \gamma_{12} = 38\%$. Each ply is checked for failure at the end of every loading increment. If the strain to failure in any direction is reached, the loading stops and the stress–strain data for that laminate is stored.

3. Model validation

The results presented in [14] allowed validation of the modelling to be performed. These quasi-static tension tests were conducted on $[\pm\theta_5]_s$ specimens, where $\theta = 15, 20, 25, 30, 45$. Table 2 presents strengths, failure strains, pseudo-ductile strains and final fibre angles for all the angle-ply laminates experimentally tested and the respective model results in each case. Representative stress–strain curves for each layup tested are plotted in Fig. 5, along with the model results. The longitudinal (ϵ_x) and transverse (ϵ_y) strains for each fibre angle are given in this figure, where it should be noted that, for clarity, the $[\pm 45_5]_s$ curves have been truncated to half the strain reached experimentally.

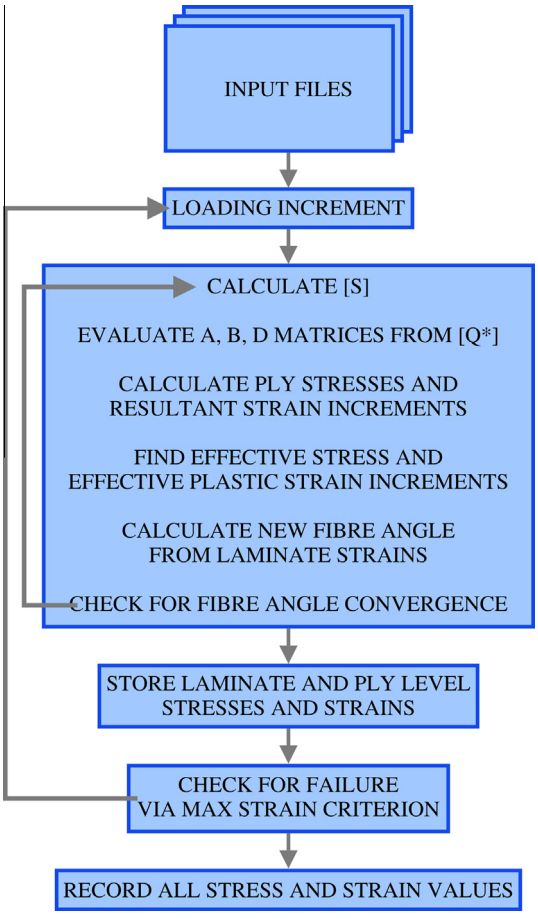

Fig. 4. Flowchart shows the steps of the analytical modelling process.

Table 2
Mean strength, strain to failure, pseudo-ductile strain and fibre rotation values for modelling and experimental results from [14]. Experimental fibre rotations are those calculated immediately prior to failure of the specimen. The coefficient of variation (CV) appears in parentheses.

		$[\pm 15_5]_s$	$[\pm 20_5]_s$	$[\pm 25_5]_s$	$[\pm 30_5]_s$	$[\pm 45_5]_s$
σ^*_x [MPa]	Test	1423 (5.5%)	1220 (2.6%)	952 (7.3%)	747 (3.7%)	390 (9.4%)
	Model	1395	1317	1051	705	303
ϵ^*_x [%]	Test	1.75 (4.2%)	2.35 (4.2%)	3.60 (6.3%)	5.72 (4.2%)	17.94 (7.9%)
	Model	1.74	2.35	3.43	4.57	16.18
ϵ_d [%]	Test	–	0.28 (24.8%)	1.22 (6.5%)	3.10 (4.7%)	13.90 (7.5%)
	Model	–	0.27	1.06	2.18	12.73
θ' [°]	Test	13.5 (0.8%)	16.8 (1.8%)	19.3 (3.2%)	22.5 (3.5%)	33.1 (1.6%)
	Model	13.4	16.2	19.4	22.9	33.6

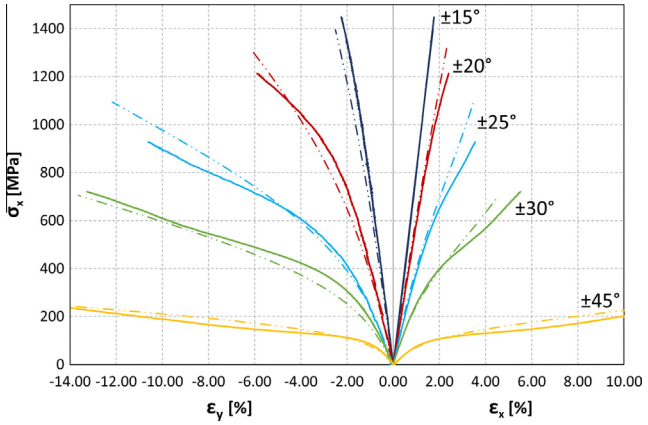

Fig. 5. The results of the modelling (dot-dash lines) for each layup are presented alongside test results (solid lines). For clarity, the output has been truncated at ϵ_x = 10% and ϵ_y = 14%.

The $[\pm 15_5]_s$ and $[\pm 20_5]_s$ specimens in particular were dominated by the fibre direction material properties. This can be seen in Fig. 5 from the low level of non-linearity developed prior to failure. The model provides a very good match to the experimental results, particularly for the $[\pm 15_5]_s$, though this loading is predominantly linear. As such, the criterion for yield was not reached and there is a complete absence of pseudo-ductility. At strains close to 2%, a slightly stiffer longitudinal response is predicted by the model for the $[\pm 20_5]_s$ layup than seen in testing. The predicted transverse strains for both layups deviate more from the experimental results. The experimental strains are more non-linear in this direction and the model under-predicts the stress, showing a divergence from the experimental after $\epsilon_y = 1\%$, though at higher strains the modelled $\pm 20^\circ$ response gives a higher stress. In both cases, the predicted strength and strain to failure values are in good agreement with the experimental. Also well-matched for this layup is the predicted amount of pseudo-ductile strain, as shown in Table 2.

Results for $[\pm 25_5]_s$ specimens show excellent correlation at low strains. Beyond 2% the modelled longitudinal result diverges, again predicting a stiffer response. Fig. 5 shows that the predicted ϵ^*_x is very similar to the experimental results, leading to the model giving a higher value of strength. This leads to a lower value of

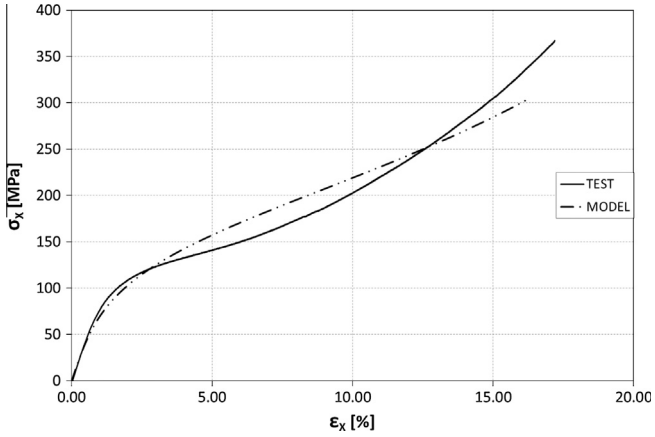

Fig. 6. The full extent of the stress–strain curve for the $[\pm 45_5]_s$ layup is shown. Modelling is indicated by dot-dash line and experimental by solid line.

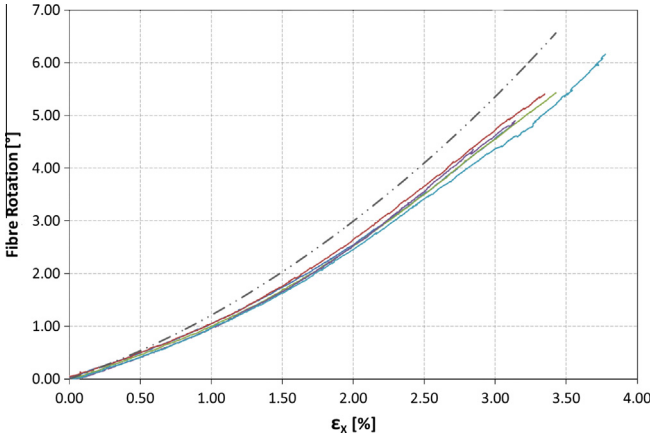

Fig. 7. Model predicted and experimental fibre rotation is presented for $[\pm 25_5]_s$ layup.

pseudo-ductility to be predicted by the model (ϵ_d = 1.06%) than is seen from the tests (ϵ_d = 1.22%). The predicted transverse strains display a similar trait to the ±20° layup — accurate initial slope and then under-prediction of the stress at low strains, followed by a stress higher than experimental. In this case, the predicted transverse strain at failure is 1.5% above the experimental value.

Experimental results for the $[\pm 30_5]_s$ laminates show a more non-linear behaviour and, as such represent a sterner test of the modelling. As can be seen in Fig. 5, the prediction is closely matched to the experimental behaviour. A similar divergence is seen at high longitudinal strains where the model predicts a stiffer response than the experimental. Dissimilarly to the $[\pm 25_5]_s$ laminate, the predicted strength of the $[\pm 30_5]_s$ matches closely to the experimental, but the strain to failure is lower. This means also that the pseudo-ductile strain is lower than seen in experiments — Table 2 showing a difference in the value ϵ_d of 0.9%. The transverse strains are more closely matched than for the ±25° layup. The predicted response shows the same divergence after 1% strain, but at higher strains the slope of the curve is well matched to the experimental. The transverse strain at failure is also adequately predicted. Table 2 also shows that the predicted fibre rotation is within 0.4° of the experimentally observed mean value. This indicates that the model is reasonably accurately predicting the stiffness of the laminate, as the amount of fibre rotation and plasticity develops. Despite not showing the complete response of the ±45° layup, Fig. 5 does indicate that the predicted longitudinal and transverse strains display very similar behaviours in relation to the experimental. To fully show the $[\pm 45_5]_s$ stress–strain behaviour, results are presented separately in Fig. 6. These specimens show strains to failure in the region of 20% and fibre reorientation in excess of 10°, leading to a large offloading of stress on to the fibres. This is manifested by a stiffening of the laminate at high strains. A low elastic modulus is exhibited, but the pseudo-ductility predicted, ϵ_d = 12.73%, is very large. Overall, the predicted response is reasonably well matched to the experimental data, though the accuracy is not as high as for the layups presented above. As with these layups, the predicted pseudo-ductile strain is lower than the experimentally attained mean value of 13.90%. Considering, however, the large amount of non-linear behaviour exhibited by this layup, the percentage difference between predicted and experimental pseudo-ductile strains are low, at just over 1%. The experimental curve shows a much more pronounced yield point at about 120 MPa, leading to a large softening of the laminate. The experimental response begins to stiffen sharply around 200 MPa, whereas the model predicts that the laminate will only stiffen at over 250 MPa. In excess of 16%, the failure strain

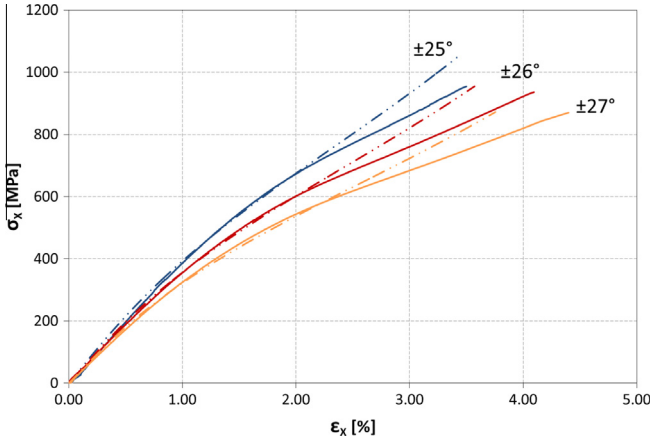

Fig. 8. Model predicted (dot-dashed lines) and experimental (solid lines) stress–strain curves are presented for the ±26°, ±27°. They are plotted alongside ±25° for comparison.

from modelling is only slightly lower than the 17% seen in experiments. The model has been unable to accurately predict the strength, predominantly due to the lower degree of stiffening at higher strains.

It is also important to assess the accuracy of the fibre rotation predicted by the modelling. Table 2 also contains the predicted and mean experimental fibre angle measured just prior to failure for each angle-ply laminate. A good agreement is in evidence for all specimens, giving confidence that the approach is accurately predicting the overall response of the laminates. Fig. 7 shows also that, with the $[\pm 25_5]_s$ response as an example, the predicted reorientation of fibres follows the experimental trend. There is an increase in fibre rotation with increasing strain. This indicates that the matrix, in agreement with modelling, has undergone some yielding and there is plastic flow, allowing the fibres to reorient. The predicted fibre rotation, for a given strain, is higher than the experimental results. This behaviour is due primarily to the difference between the predicted and experimental transverse strains. The larger change in fibre angle also provides some insight into the stiffer predicted stress–strain responses discussed above. It is clear that, though the plasticity model reduces the stiffness of the laminate via the terms of the $[Q_p]$ matrix, the method employed to calculate fibre rotation causes a great deal of the stiffness to be maintained, counteracting the effects of the plasticity.

4. Potential for pseudo-ductility

Inspection of Fig. 5 shows that there is an interesting region between ±25° and ±30°. Both the modelling and experimental results for the $[\pm 25_5]_s$ layup show a high strength but limited pseudo-ductility. Whereas the $[\pm 30_5]_s$ results display larger pseudo-ductility but the strength is reduced by 30%. This suggests that between these fibre angles, it will be possible to maintain more of the stiffness and strength while increasing the level of pseudo-ductility exhibited by the laminate. To investigate this, predictions were made for $[\pm 26_5]_s$ and $[\pm 27_5]_s$ laminates. These modelling results are presented in Fig. 8, alongside the results for $[\pm 25_5]_s$ for ease of comparison.

4.1. Experimental procedure

To further evaluate the performance of the modelling, quasi-static tensile testing was performed on $[\pm 26_5]_s$ and $[\pm 27_5]_s$ specimens. Batches of five were tested in each case and all were loaded to complete failure of the specimen. Tests were performed under displacement control at a rate of 2 mm/min, using an Instron 8872 hydraulically-actuated test machine. Specimen dimensions were kept consistent with those used in [14], with a gauge length of 150 mm, width of 15 mm and glass fibre-epoxy end tab region of 40 mm. Three-point thickness measurements confirmed that the cured ply thickness was consistent with previous tests, at 0.03 mm (CV = 0.47%). All longitudinal and transverse strain data was recorded using an Imetrum video extensometry system.

The experimentally observed failures exhibited by each specimen were all initiated within the gauge length. Inspection of the failed specimens showed that any damage was local to the failure surface. Failure was driven by fibre fracture and splitting, with a complete absence of delaminations.

4.2. Correlation with modelling

The modelling of $[\pm 26_5]_s$ and $[\pm 27_5]_s$ show, in Fig. 8 and Table 3, excellent correlation with the experimental results at low strains. At strains in excess of 2%, both predictions exhibit a similar divergence as that seen in Fig. 5, where a stiffer response up to failure is predicted. In contrast to the prediction for the $[\pm 25_5]_s$, which shows a higher strength but similar failure strain to the experimental results, the predicted failure strains for both $[\pm 26_5]_s$ and $[\pm 27_5]_s$ are surpassed by the experimental. The values predicted for strength, however, are well matched to the experimental for these layups. This leads also to a larger experimental pseudo-ductile strain than predicted.

Most notably, while the modelling predicts relatively small increases in strain to failure, but large reductions in strength, the experimental behaviour is seen to be somewhat different. Fig. 8 shows that there is very little loss in strength between the $[\pm 25_5]_s$ (σ_x^* = 952 MPa) and $[\pm 26_5]_s$ (σ_x^* = 936 MPa) specimens. This occurs, however, with almost a 20% increase in strain to failure for the $[\pm 26_5]_s$. This is a very interesting result, as it shows that a layup with a fibre angle of ±26° can achieve similar strengths to one that is initially stiffer and also reach higher strains. The increased strain to failure also goes to extend the pseudo-ductility possible, as shown in Table 3.

Table 3
Mean strength, strain to failure, pseudo-ductile strain and fibre rotation values for modelling and experimental results for $[\pm 26_5]_s$ and $[\pm 27_5]_s$. The coefficient of variation (CV) appears in parentheses beside the relevant experimental value.

		$[\pm 25_5]_s$	$[\pm 26_5]_s$	$[\pm 27_5]_s$
σ_x^* [MPa]	Test	952 (7.3%)	936 (2.6%)	870 (2.6%)
	Model	1051	955	872
ϵ_x^* [%]	Test	3.60 (6.3%)	4.10 (5.0%)	4.40 (4.4%)
	Model	3.43	3.57	3.76
ϵ_d [%]	Test	1.22 (6.5%)	1.47 (12.0%)	1.89 (7.8%)
	Model	1.02	1.20	1.40
θ' [°]	Test	19.3 (3.2%)	18.9 (7.0%)	19.7 (3.5%)
	Model	19.4	19.4	20.3

5. Exploration of parameters governing pseudo-ductility

The model has been shown to be able to predict, with reasonable accuracy, the stress–strain behaviour of thin ply angle-ply laminates. With this analytical approach in place, it is then possible to explore the factors that govern the non-linearity of the angle-ply response. Using the micromechanical model, which defines the plastic behaviour of the composite, the effects of changing the resin properties on parameters, such as pseudo-ductile strain, yield stress and strength, have been investigated. As discussed above, the effective plastic strain in the matrix is related to effective stress by the values of β and n as per Eq. 3. If a range of values for β and n are picked to describe hypothetical effective plastic behaviours of the resin, the influence these have on the composite stress–strain response can be determined by following the process laid out above.

In addition to the value of $\beta = 3.5 \times 10^{-33}$ already used, two further values of 1×10^{-27} and 1×10^{-47} have been chosen and are coupled with the following ranges of values for n:

- 1×10^{-27} — 3.05; 3.12; 3.17; 3.21; 3.24; 3.28.
- 3.5×10^{-35} — 3.65; 3.75; 3.80; 3.83; 3.86; 3.90.
- 1×10^{-47} — 5.55; 5.60; 5.63; 5.67; 5.73; 5.80.

The values given above allow the shape of the power law to be controlled, in terms of the onset and severity of the matrix yielding. Examples of this control are presented in Fig. 9, which highlights the sensitivity of the $\bar{\sigma}_M - \bar{\epsilon}_M^p$ behaviour to the values of β and n. These β-n combinations give a realistic range of matrix yield behaviours and aim to show the influence of the matrix yield on the composite response, which could provide guidance for future selection of materials. For reference, the values of β and n used for the Skyflex matrix response are also presented in Fig. 9. The resin elastic modulus has been kept constant throughout, though the fibre volume fraction has been increased to 50%, which is a more representative value than the relatively low 42% the Skyflex material possesses. As discussed above, fibre angles

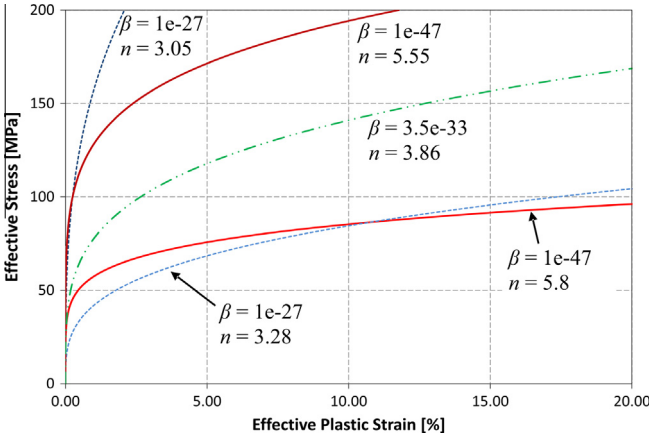

Fig. 9. Examples of $\beta - n$ combinations are presented. The sensitivity of the matrix plasticity to each parameter is clear, as small changes in n lead to large changes in the post-yield behaviour.

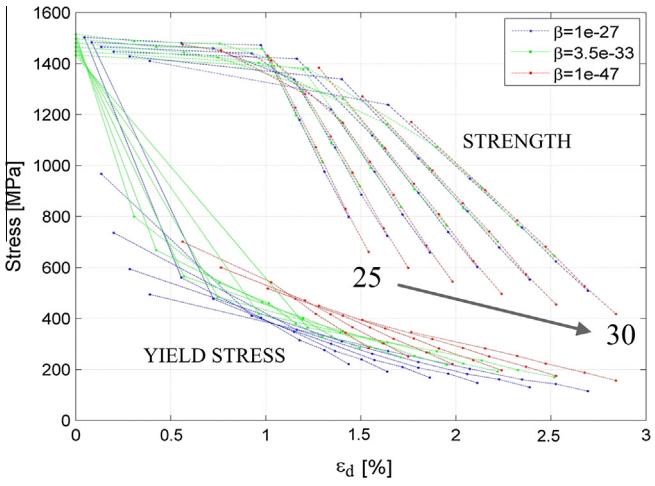

Fig. 10. Strength and "yield" stress plotted against pseudo-ductile strain, showing the effect of varying the values β and n. Each line denotes a fibre angle between $\pm 25^{\circ}$ and $\pm 30^{\circ}$, while the dot markers indicate increasing values of n left—right.

between $\pm 25^{\circ}$ and $\pm 30^{\circ}$ have been shown to exhibit the most promising pseudo-ductility. In 1° increments, these angles have been modelled with each value of β and six values of n. The values of "yield" stress, pseudo-ductile strain and strength are recorded for each layup and β, n combination and the results are presented in Fig. 10. The "yield" stress and strength are plotted against pseudo-ductile strain, where each line represents a layup and the dot markers along it show, from left to right, the effect of increasing the value of n — effectively increasing the extent of yield.

Apparent from this plot is the similarity between results from each value of β. Altering this does not greatly affect the results at the highest values of n, particularly in the case of the laminate strengths. The "yield" is seen to be more affected. "Yield" stress is seen to increase with reducing β for a given value of pseudo-ductile strain. This is shown by the clear blue, green, red separation on the plot. Clearly, a compromise between strength, "yield" stress and pseudo-ductility has to be made. For each fibre angle, there is a point at which the strength decreases sharply. This shows that the more exaggerated the yielding of the matrix is, the more pseudo-ductile strain can be achieved, but at the cost of the strength of the laminate.

Overall, Fig. 10 shows that it is possible to tailor the response of these laminates for strength, "yield" and pseudo-ductile strain. For example, if a pseudo-ductile strain of 1% is desired, with careful selection of fibre angle, a strength of 1000 MPa and a "yield" stress of 500 MPa can be reached.

6. Conclusions

The analytical modelling approach described in Section 2 has shown that the stress–strain behaviour of thin ply angle-ply laminates can be adequately predicted using a model taking account of matrix plasticity and fibre rotation. The model has been validated against experimental data from monotonic tensile tests performed previously on $[\pm\theta_5]_s$, where $\theta = 15$, 20, 25, 30 and 45. Excellent correlation of the stress–strain response has been shown below 2% strain, before a small divergence between prediction and experimental. The modelling predicted a stiffer response at high strains for all layups, though the mean percentage difference in strength was modest at 7.7%. The predicted longitudinal strains to failure were well-matched for angles of $\pm 25^{\circ}$ and less, though at higher angles the predictions turned out to be conservative, leading to an mean percentage difference of 9.5% across all fibre angles.

The modelling has shown sufficient accuracy to allow further predictions to be performed to explore the potential of these laminates. Predictions and subsequent experimental testing of $[\pm 26_5]_s$ and $[\pm 27_5]_s$ laminates yielded promising pseudo-ductile results. The modelling of $\pm 26^{\circ}$ exhibited a strength of 955 MPa, pseudo-ductile strain of 1.20% and strain to failure of 3.76%. The experimental strain to failure, and so the pseudo-ductile strain, surpassed predictions, reaching 4.10% and 1.47% respectively.

The factors governing the non-linear stress–strain response of these thin ply angle-ply laminates has also been investigated. By varying the plastic properties of the matrix, it has been possible to show, for fibre angles between $\pm 25^{\circ}$ and $\pm 30^{\circ}$, how the strength and "yield" stress interact with the pseudo-ductile strain. The method shows clearly how the laminate behaviour can be tailored to achieve a desired pseudo-ductility. Ultimately, with sufficient data for available materials, this modelling technique can give a straightforward analysis of fibre — matrix combinations in order to develop future thin ply composites that display a prescribed non-linear behaviour.

Acknowledgements

This work is part of the EPSRC Programme Grant EP/I02946X/1 on High Performance Ductile Composite Technology in collaboration with Imperial College, London and is financially supported by Grant No. EP/G036772/1 (as part of the ACCIS Centre for Doctoral Training).

References

[1] Sasayama H, Kawabe K, Tomoda S, Ohsawa I, Kageyama K, Ogata N. Effect of lamina thickness on first ply failure in multidirectionally laminated composites. In: Proceedings of 8th Japan International SAMPE symposium and exhibition, Tokyo: 2003, p. 18–21.
[2] Sihn S, Kim R, Kawabe K, Tsai S. Experimental studies of thin-ply laminated composites. Compos Sci Technol 2007;67:996–1008.
[3] Guillamet G, Turon A, Costa J, Renart J, Linde P, Mayugo JA. Damage occurrence at edges of non-crimp-fabric thin-ply laminates under off-axis uniaxial loading. Compos Sci Technol 2014;98:44–50.
[4] Yokozeki T, Aoki Y, Ogasawara T. Experimental characterization of strength and damage resistance properties of thin-ply carbon fiber/toughened epoxy laminates. Compos Struct 2008;82:382–9.
[5] Yokozeki T, Aoki T, Ogasawara T, Ishikawa T. Effects of layup angle and ply thickness on matrix crack interaction in contiguous plies of composite laminates. Compos Part A Appl Sci Manuf 2005;36:1229–35.
[6] Ogihara S, Nakatani H. Effect of ply thickness on mechanical properties in CFRP angle-ply laminates. In: Proceedings of ECCM-15, Venice; June 2012.
[7] Amacher R, Cugnoni J, Botsis J, Sorensen L, Smith W, Dransfeld C. Thin ply composites: experimental characterization and modeling of size-effects. Compos Sci Technol 2014;101:121–32.
[8] Arteiro A, Catalanotti G, Xavier J, Camanho PP. Notched response of non-crimp fabric thin-ply laminates. Compos Sci Technol 2013;79:97–114.
[9] Arteiro A, Catalanotti G, Xavier J, Camanho PP. Large damage capability of non-crimp fabric thin-ply laminates. Compos Part A Appl Sci Manuf 2014;63:110–22.
[10] Yokozeki T, Kuroda A, Yoshimura A, Ogasawara T, Aoki T. Damage characterization in thin-ply composite laminates under out-of-plane transverse loadings. Compos Struct 2010;93:49–57.
[11] Wisnom MR. The effect of fibre rotation in ±45 tension tests on measured shear properties. Composites 1995;26:25–32.
[12] Herakovich CT, Schroedter R, Gasser A, Guitard L. Damage evolution in [±45]s laminates with fiber rotation. Compos Sci Technol 2000;60:2781–9.
[13] Ladeveze P, LeDantec E. Damage modelling of the elementary ply for laminated composites. Compos Sci Technol 1992;43:257–67.
[14] Fuller JD, Wisnom MR. Pseudo-ductility and damage suppression in thin ply CFRP angle-ply laminates. Compos Part A Appl Sci Manuf 2014;69:64–71.
[15] Herakovich CT. Influence of layer thickness on the strength of angle-ply laminates. J Compos Mater 1982;16:216–27.
[16] Sun CT, Chen JL. A simple flow rule for characterizing nonlinear behavior of fiber composites. J Compos Mater 1989;23:1009–20.
[17] Sun CT, Chen JL. A micromechanical model for plastic behavior of fibrous composites. Compos Sci Technol 1991;40:115–29.
[18] Sun CT, Yoon K. Elastic–plastic analysis of AS4/PEEK composite laminate using a one-parameter plasticity model. J Compos Mater 1992;26:293–308.
[19] Winn VM, Sridharan S. An investigation into the accuracy of a one-parameter nonlinear model for unidirectional composites. J Compos Mater 2001;35:1491–507.
[20] Mitsubishi Rayon. Mitsubishi Rayon Pyrofil Carbon Fibres.pdf; 2013.